Angewandte Chemie
Eine Zeitschrift der Gesellschaft Deutscher Chemiker

Supporting Information

69451 Weinheim, Germany

Ultrafast X-ray solution scattering reveals a new reaction intermediate in the photolysis of $Ru_3(CO)_{12}$**

Qingyu Kong[†], Jae Hyuk Lee[‡], Anton Plech[¶], Michael Wulff[†], Hyotcherl Ihee[‡*], Michel H. J. Koch[§]

[†]*European Synchrotron Radiation Facility, 6 Rue Jules Horowitz, BP220, F-38043 Grenoble Cedex, France*

[‡]*Center for Time-Resolved Diffraction, Department of Chemistry (BK21), KAIST, Daejeon, 305-701, Republic of Korea*

[¶]*Fachbereich Physik der Universität Konstanz, Universitätsstrasse. 10, D-78457 Konstanz, Germany*

[§]*European Molecular Biology Laboratory, Hamburg Outstation, EMBL c/o DESY, Notkestrasse 85, D-22603 Hamburg, Germany*

Experimental Section

Experimental

$Ru_3(CO)_{12}$ (99%) (Sigma-Aldrich) and spectroscopic grade cyclohexane (Sigma-Aldrich) (>99.5%) were used without further purification to prepare a ~3 mM solution which was filtered before the measurements. The experimental setup of the ID09B beamline at the European Synchrotron Radiation Facility (ESRF) has been described in detail elsewhere[S1-S4]. Briefly, a 100 fs (fwhm) optical pulse at 390 nm stretched to 2 ps by passing the beam through two 30-cm long SF-10 prisms to lower the peak power and avoid multiphoton absorption, was used to excite the $Ru_3(CO)_{12}$ molecules dissolved in cyclohexane. The relaxation of the excited molecules was monitored with a delayed 100 ps (fwhm) X-ray pulse, selected with a synchronized mechanical chopper rotating at a frequency of 986.3 Hz, the 360^{th} sub-harmonic of the orbit frequency at ESRF. A time resolution of ~50 ps was achieved by laser time-slicing, i.e. using co-linear laser and X-ray beams and scanning the laser pulse position in small steps inside the (longer) X-ray pulse. For time zero, for example, the downstream part of the X-ray pulse becomes a 50 ps long step-truncated Gaussian pulse[S5]. A polychromatic X-ray beam centered at 17.9 keV (0.69 Å) with 5×10^8 photons per pulse from the single-harmonic U17 undulator was focused into an elliptical 100×60 μm^2 (FWHM) spot on the sample by a toroidal mirror. A sapphire nozzle which produces a liquid sheet of 0.3 mm thick sheet of liquid was used to cycle the solution (300 mL) in the measurement cell at a speed of approximately 3 m/s.

To follow the kinetics of the transient intermediates, a series of X-ray scattering patterns was collected with an area detector (MarCCD, Mar USA, Evanston, IL) at time delays of -3 ns, -100 ps, 20 ps, 50 ps, 70 ps, 100 ps, 200 ps, 300 ps, 500 ps, 1 ns, 3 ns, 5 ns, 10 ns, 30 ns, 50 ns, 100 ns, 300 ns, 700 ns, and 1 μs relative to the center of the laser excitation pulse. The difference scattering intensities $\Delta S(q,t)$, obtained by azimuthal

integration of the difference CCD images, were amplified at high q by multiplying them by q and the $q\Delta S(q,t)$ patterns were used in all further calculations. The temporal intensity of the 100-ps long X-ray pulse was taken into account in the normalization of the X-ray signal, i.e. using only that part of the X-ray pulse that probes the system after photo-excitation. Nominal time delays of 20 ps, 50 ps, and 70 ps correspond to the effective time delays of 40 ps, 60 ps, and 75 ps, respectively, when the widths of the laser (2 ps) and X-ray (100 ps) pulses are taken into account.

Based on the absorption spectrum for cyclohexane (Fig. S1), the impulsive heating of pure cyclohexane was excited by a near infrared laser pulse at 1700 nm, produced with the OPO-OPA system (TOPAS). The temperature and density changes were deduced from the measured signal as explained previously[S6] and used in the least-squares fits.

Quantum chemical (DFT) calculations

To assist the data analysis and judge the relative stability of the possible photofragmentation products of $Ru_3(CO)_{12}$, the geometries and relative energies of sixteen possible transient intermediates shown in Fig. S2 were calculated and optimized with density functional theory (DFT), as implemented in the Gaussian 03 program[S7]. The Becke three-parameter hybrid functional with the Lee-Yang-Parr correlation corrections (B3LYP) level was used[S8-S9]. The all electron basis set 6-311+G(d) for C and O, and the Stuttgart RSC 1997 effective core potential for Ru were used in the DFT calculations. The potential energy levels of the three transient intermediates remaining after the least squares fit (Fig. 2A) including all the candidate molecules considered in this work are shown in Fig. S2 and the energy levels of selected transient intermediates along the photoreaction pathway of the photolysis of $Ru_3(CO)_{12}$ are indicated in Fig. S3. We have found three stable $Ru_3(CO)_{10}$ isomers (Intermediates 3, 3A, and 3B). When we considered a $Ru_3(CO)_{10}$ isomer with two CO cleaved off from different Ru as a starting

geometry, DFT optimization yielded intermediate 3A and 3B with bridging CO(s). Other possible geometries were also considered, but the optimized structures have imaginary frequencies indicating that they are not stable structures, but transition states on the potential energy surface. The energies of all candidate molecules relative to the initial molecule are given in Table S1. Fig. S4 shows the solute-only term calculated by the Debye formula for all candidate species.

Methods used for MD simulations and the extraction of the cage structure have been described elsewhere[S2-S3]. The solute/solvent interactions (cage structure) were obtained by MD simulation using the MOLDY program[S10]. A six-center Lennard-Jones potential was used for cyclohexane as described previously[S11], and the intermolecular all-atom Lennard-Jones potential was employed for the solute molecule with the following values for the depth of the potential well (ε in kJM^{-1}) and the equilibrium distance (σ in Å): Ru-Ru: ε = 0.105, σ= 2.940; C-C: ε = 0.758, σ= 3.861; O-O: ε = 0.731, σ= 3.083. All molecules were treated as rigid and no further refinement was made.

Global fitting analysis and kinetics of various solute molecules

The scattered intensity from a solution has three contributions: the scattering from the solute molecule itself, the bulk solvent, and the solvent/solute cross-term (cage). The bulk solvent response to a temperature and density change caused by the reaction itself can be described with the temperature and density derivatives determined by impulsive heating of the solvent by near infrared (NIR) laser pulses as follows[S6]:

$$\Delta S_{solvent}(q,t) = \left(\frac{\partial S}{\partial T}\right)_{\rho} \Delta T(t) + \left(\frac{\partial S}{\partial \rho}\right)_{T} \Delta\rho(t)$$

Molecular Dynamics (MD) simulation provides the scattering intensities from solutes and solute-solvent cross-terms. Hence the total scattering intensity is composed of the sum of all scattering intensities[S2]:

$$\Delta S_{theory}(q,t) = \left[\sum_k f_k(t) S_k(q) - S_g(q) \sum_k f_k(0) \right] + \left(\frac{\partial S}{\partial T} \right)_\rho \Delta T(t) + \left(\frac{\partial S}{\partial \rho} \right)_T \Delta \rho(t)$$

where k is the index of the solute (reactant, product, and intermediates), f_k the fraction of molecules in k, $S_k(q)$ is the solute-related (the solute-only term plus the solute/solvent cross term) scattering intensity of species k, and $S_g(q)$ is the scattering intensity of the reactants. For comparison with the experimental data, the model (theoretical) curves were convoluted with the wavelength profile of the incident X-ray beam after correction for absorption.

To extract a reaction mechanism from these results, a reaction model including all reasonable candidate reaction pathways was used as shown in Figure 3A. Based on this model, the time course of the concentration changes of various chemical species can be calculated by integrating the differential rate equations. Integrating the rate equations provides f_k, the fraction of each molecule, to be used to construct the theoretical scattering signal. The strategy in least-squares fitting the theoretical scattering curves to the experimental data is to minimize the total χ^2 iteratively in a global-fitting procedure simultaneously minimizing the curves at all positive time delays[S2]:

$$\chi^2 = \sum_{j=\text{time delay}} \chi_j^2$$

$$\chi_j^2 = \sum_i \left(\frac{\Delta S_{\text{theory}}(q_i, t_j) - \Delta S_{\text{experimental}}(q_i, t_j)}{\sigma_{i,j}} \right)^2$$

where $\sigma_{i,j}$ is the error bar on the experimental curves calculated as the standard deviation of the different repetitions of a given time-delay. The fitting parameters are the rate-constants. The occupancies of the respective species enter the fitting under the

restriction that the number of atoms is conserved. The other fitting parameter is the laser beam size, which is used to optimize the time-constant of thermal expansion.

Hydrodynamics of the bulk solvent

As the excited $Ru_3(CO)_{12}$ molecule relaxes along the potential energy surface, it might either form the intermediates 1 and 2 plus $Ru_3(CO)_{10}$ (intermediate 3), or it might recoil back to the ground state through vibrational cooling, the excess energy is released as heat to the surrounding solvent. The time dependence of the thermodynamic quantities such as the changes in density $\Delta\rho(t)$ and temperature $\Delta T(t)$ of the bulk solvent can be followed as the heat is released from the solutes and propagates through the solution. Figure S5 shows the temporal variations of $\Delta\rho(t)$ and $\Delta T(t)$ of the bulk solvent after laser excitation. The density decreases by 0.8 kg/m^3 (0.10%) in 1 μs after the thermal expansion is completed, with an associated temperature change of 0.84 K. While the global fitting analysis provides $\Delta\rho(t)$ and $\Delta T(t)$[S2], the same information can be extracted even without using the global fitting analysis as follows. The density change of the solution can be obtained from the sine-Fourier transforms of the measured difference scattering intensities $\Delta S(q,t)$ through the following equations[S12,S13]:

$$\Delta R(r,t) = \frac{10^{30}}{N_A} M_{C_6H_{12}} \frac{1}{2\pi^2 r} \int_0^\infty \frac{q\Delta S(q,t)}{\sum_{i=j} f_i(q) f_j(q)} \sin(qr) e^{-(\alpha q)^2} dq$$

$$\Delta\rho(t) = -\lim_{r\to 0} \Delta R(r,t)$$

where N_A is Avogadro´s number, M_{C6H12} is the mass of one cyclohexane molecule, and $\sum_{i=j} f_i(q) f_j(q) = \sum f_i^2(q)$ is the sharpening factor. The density change $\Delta\rho(t)$ can be extracted from the small-r (r = 10/q_{max}) portion of the measured $\Delta R(r,t)$, while the

temperature change ($\Delta T(t)$) can be calculated via thermodynamic relations which have been described in detail previously[S12].

TABLE S1: Energies (kJ mol^{-1}) of the different intermediates in Fig. S2 relative to the ground state of $Ru_3(CO)_{12}$, obtained by DFT calculations.

Species	Relative energies (kJ mol^{-1})
$Ru_3(CO)_{12}$_ground state	0.0
$Ru_3(CO)_{12}^*$_excited state	306.1
$Ru_3(CO)_{12}$ intermediate 1	117.1
$Ru_3(CO)_{12}$ intermediate 1A	128.2
$Ru_3(CO)_{12}$ intermediate 1B	151.3
$Ru_3(CO)_{11}$ axial CO loss intermediate 2+ CO	104.2
$Ru_3(CO)_{11}$ equatorial CO loss intermediate 2A +CO	141.2
$Ru_3(CO)_{10}$ intermediate 3 + 2CO	240.9
$Ru_3(CO)_{10}$ intermediate 3A + 2CO	308.0
$Ru_3(CO)_{10}$ intermediate 3B+ 2CO	310.2
$Ru_3(CO)_9$ + 3CO	436.0
$Ru_2(CO)_9$ + 3CO + Ru	716.9
$Ru_2(CO)_9$ + $Ru(CO)_3$	236.9
$Ru_2(CO)_8$ + 4CO + Ru	828.1
$Ru_2(CO)_8$ + $Ru(CO)_4$	168.4
$Ru_2(CO)_6$ eclipsed + 6CO + Ru	1064.7
$Ru_2(CO)_6$ eclipsed +$Ru(CO)_5$ + CO	299.9
$Ru_2(CO)_6$ bridged +6CO +Ru	1116.6
$Ru_2(CO)_6$ bridged +$Ru(CO)_5$ + CO	351.7

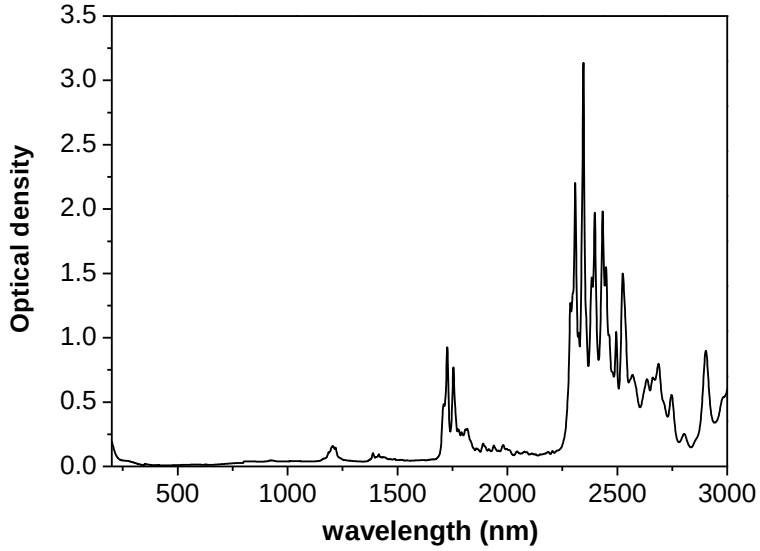

Fig. S1. Infrared absorption spectrum of pure cyclohexane. The band around 1700 nm corresponds to over-tone excitations of C-H bonds.

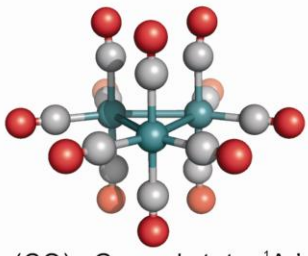

$Ru_3(CO)_{12}$ Ground state, $^1A_1$'

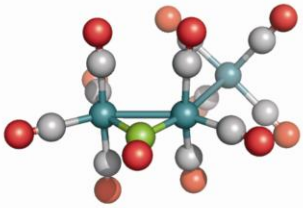

$Ru_3(CO)_{12}$ Intermediate 1, ^1A

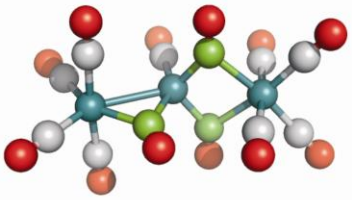

$Ru_3(CO)_{12}$ Intermediate 1A, ^1A

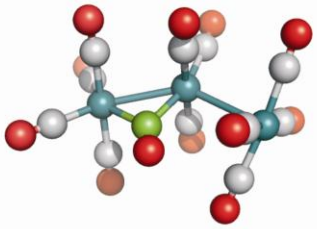

$Ru_3(CO)_{12}$ Intermediate 1B, ^1A

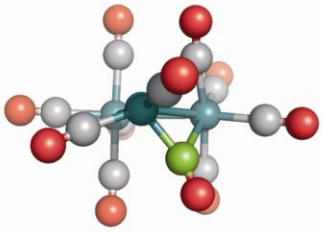

$Ru_3(CO)_{11}$ axial CO loss Intermediate 2, ^1A

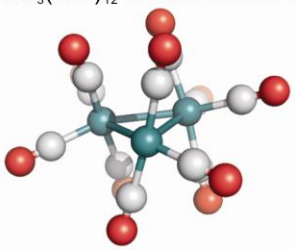

$Ru_3(CO)_{11}$ equatorial CO loss Intermediate 2A, ^1A

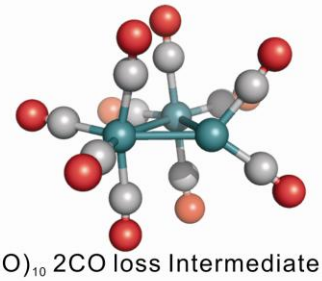

$Ru_3(CO)_{10}$ 2CO loss Intermediate 3, ^1A

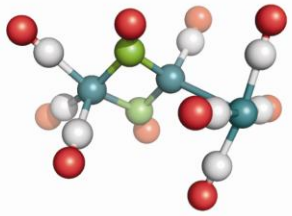

$Ru_3(CO)_{10}$ 2CO loss Intermediate 3A, ^1A

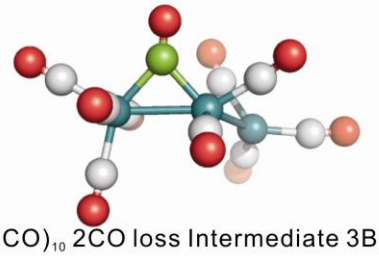

$Ru_3(CO)_{10}$ 2CO loss Intermediate 3B, ^1A

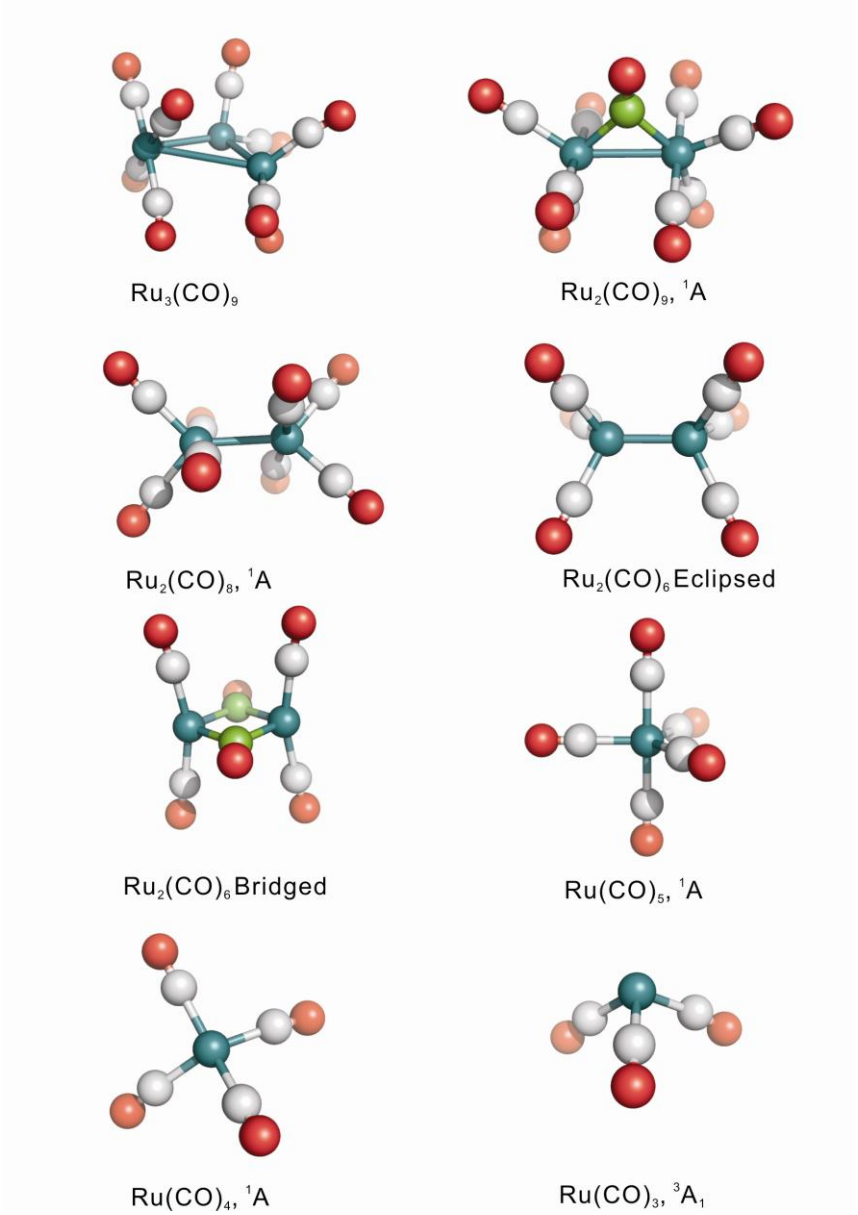

Fig. S2 Geometries obtained by DFT calculations of the parent molecule and various intermediates considered in this work. Ru, C, and O atoms are colored in cyan, gray, and red, respectively. To distinguish bridging carbonyls, their carbon atoms are colored in green. Symbols after the name correspond to the symmetry. The B3LYP level with the 6-311+G(d) basis set for C and O, Stuttgart RSC 1997 ECP for Ru were used in the calculation. The observed intermediates are labelled in bold characters.

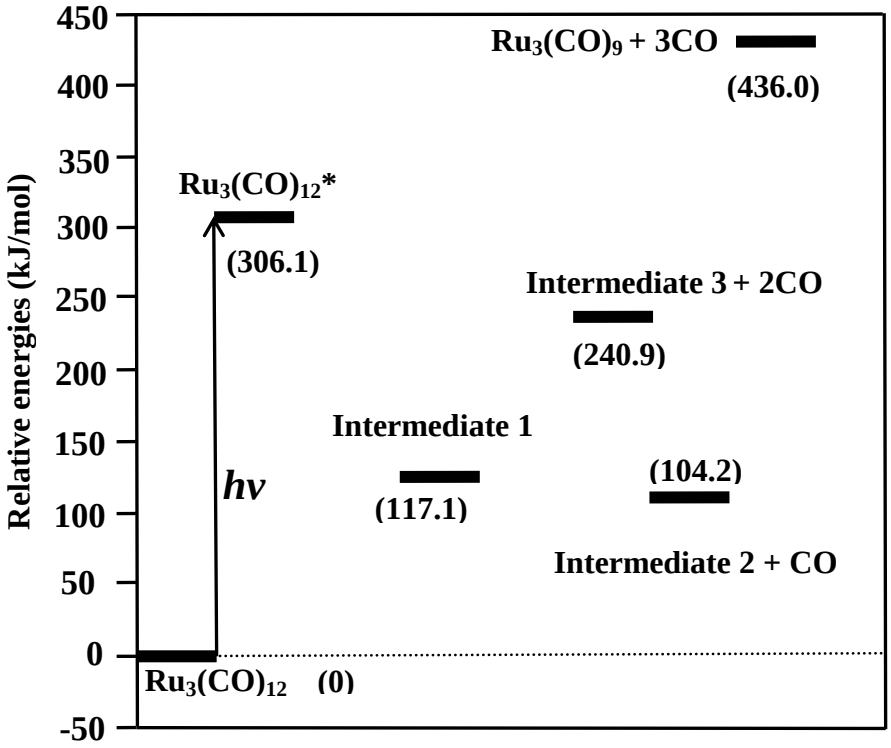

Fig. S3. Potential energy levels relative to the ground state of $Ru_3(CO)_{12}$ for selected transient intermediates from Fig. S2. Energies were calculated at the B3LYP level with the 6-311+G(d) basis set for C and O, Stuttgart RSC 1997 ECP for Ru and subjected to ZPE correction.

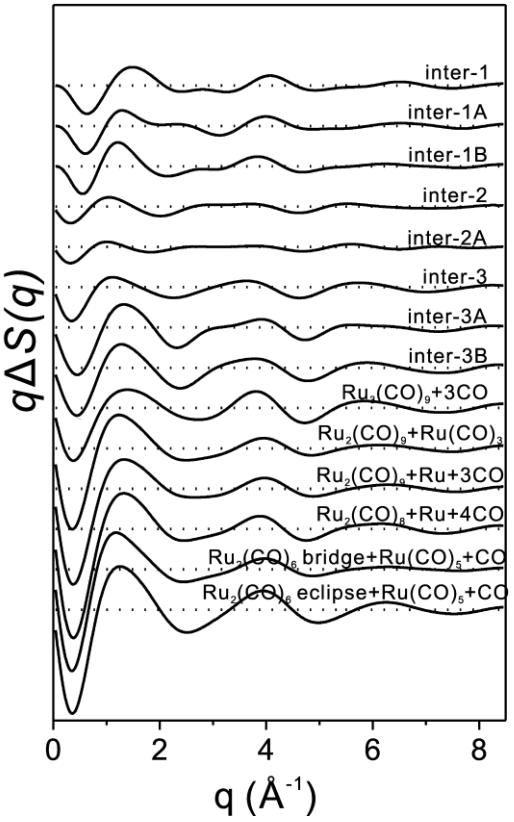

Fig. S4. Theoretical solute-only curves for the candidate intermediates shown in Table S1.

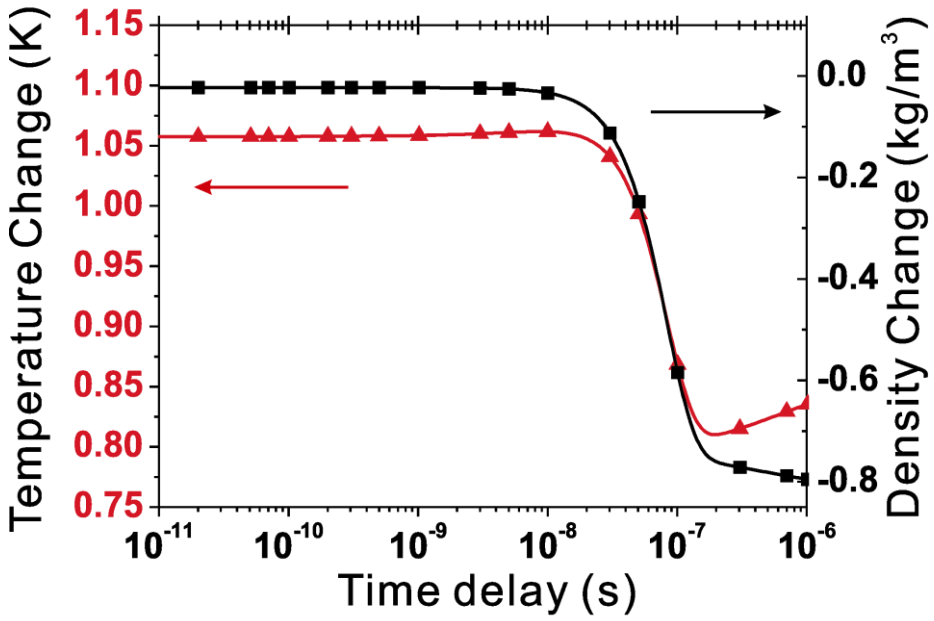

Fig. S5. Time course of the change in solvent density ($\Delta\rho(t)$), and solvent temperature ($\Delta T(t)$). The arrows point to the ordinate for each curve.

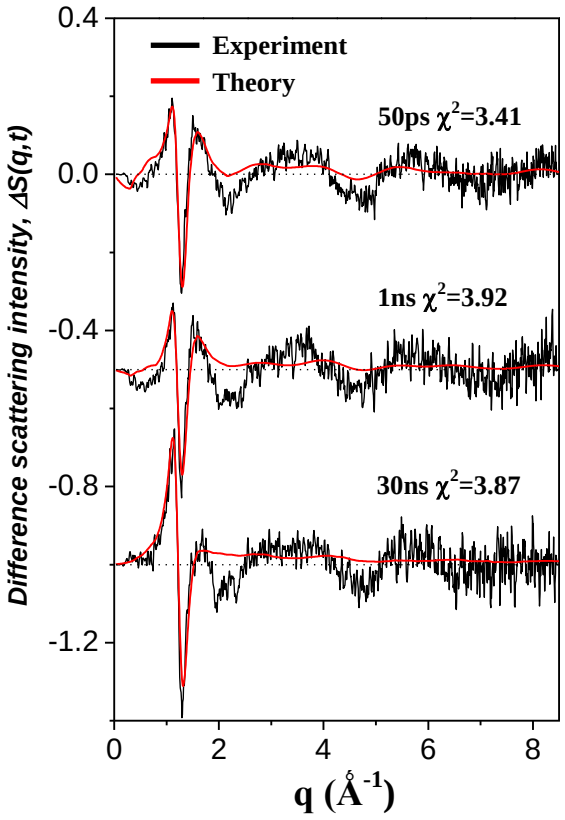

Fig. S6. Least squares fit to the difference scattering intensities ($q\Delta S(q,t)$) over the entire q-range at selected time delays including intermediates 1 and 2 only. These curves should be compared with the corresponding ones in Fig. 2a in the report.

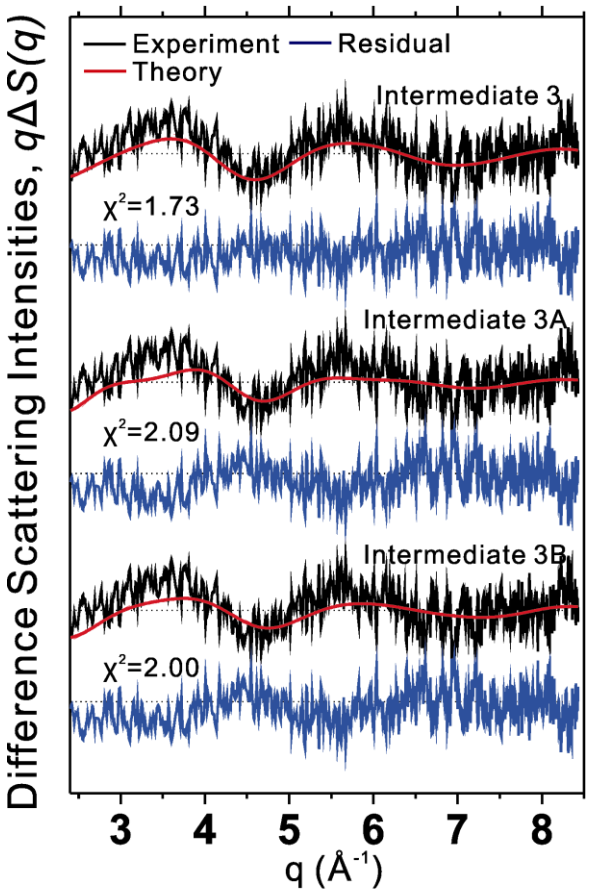

Fig. S7. Determination of the photoproducts and characterization of intermediate 3. Experimental (black) and theoretical (red) difference scattering intensities $q\Delta S(q)$ at 10 ns for three candidate intermediates (Intermediate 3, Intermediate 3A, Intermediate 3B) for $Ru_3(CO)_{10}$ are shown. Intermediate 3 is in best agreement with the experiment. When the three intermediates are included in the fit, the concentrations of the other two intermediates converge to zero.

References

15. T. K. Kim, M. Lorenc, J. H. Lee, M. Russo, J. Kim, M. Cammarata, Q. Y. Kong, S. Noel, A. Plech, M. Wulff, H. Ihee, *Proc. Nat.l Acad. Sci. USA.* **2006**, 103, 9410.

17. M. Cammarata, M. Lorenc, T. K. Kim, J. H. Lee, Q. Y. Kong, E. Pontecorvo, M. Lo Russo, G. Schiro, A. Cupane, M. Wulff, H. Ihee, *J. Chem. Phys.* **2006**, 124. 124504.

S1. A. Plech, M. Wulff, S. Bratos, F. Mirloup, R. Vuilleumier, F. Schotte, P. A. Anfinrud, *Phys. Rev. Lett.* **2004**, 92, 125505.

S2. H. Ihee, M. Lorenc, T. K. Kim, Q. Y. Kong, M. Cammarata, J. H. Lee, S. Bratos, M. Wulff, *Science* **2005**, 309, 1223.

S3. T. K. Kim, M. Lorenc, J. H. Lee, M. Russo, J. Kim, M. Cammarata, Q. Y. Kong, S. Noel, A. Plech, M. Wulff, H. Ihee, *Proc. Nat.l Acad. Sci. USA.* **2006**, 103, 9410.

S4. Q. Y. Kong, M. Wulff, J. H. Lee, S. Bratos, H. Ihee, *J. Am. Chem. Soc.* **2007**, 129, 13584.

S5. R. Neutze, R. Wouts, *J.Synchrotron Rad.* **2000**, 7, 22.

S6. M. Cammarata, M. Lorenc, T. K. Kim, J. H. Lee, Q. Y. Kong, E. Pontecorvo, M. Lo Russo, G. Schiro, A. Cupane, M. Wulff, H. Ihee, *J. Chem. Phys.* **2006**, 124. 124504.

S7. Gaussian03 (Revision C.02) M. J. Frisch, H. B. Schlegel, G. E. Scuseria, M. A. Robb, J. R. Cheeseman, J. A. Montgomery, Jr., T. Vreven, K. N. Kudin, J. C. Burant, J. M. Millam, S. S. Iyengar, J. Tomasi, V. Barone, B. Mennucci, M. Cossi, G. Scalmani, N. Rega, G. A. Petersson, H. Nakatsuji, M. Hada, M. Ehara, K. Toyota, R. Fukuda, J. Hasegawa, M. Ishida, T. Nakajima, Y. Honda, O. Kitao, H. Nakai, M. Klene, X. Li, J. E. Knox, H. P. Hratchian, J. B. Cross, V. Bakken, C. Adamo, J. Jaramillo, R. Gomperts, R. E. Stratmann, O. Yazyev, A. J. Austin, R. Cammi, C. Pomelli, J. W. Ochterski, P. Y. Ayala, K. Morokuma, G. A. Voth, P. Salvador, J. J. Dannenberg, V. G. Zakrzewski, S. Dapprich, A. D. Daniels, M. C. Strain, O. Farkas,

D. K. Malick, A. D. Rabuck, K. Raghavachari, J. B. Foresman, J. V. Ortiz, Q. Cui, A. G. Baboul, S. Clifford, J. Cioslowski, B. B. Stefanov, G. Liu, A. Liashenko, P. Piskorz, I. Komaromi, R. L. Martin, D. J. Fox, T. Keith, M. A. Al-Laham, C. Y. Peng, A. Nanayakkara, M. Challacombe, P. M. W. Gill, B. Johnson, W. Chen, M. W. Wong, C. Gonzalez, and J. A. Pople, in Gaussian, Inc, Wallingford CT, 2004.

S8. A. D. Becke, *J. Chem. Phys.* **1993**, 98, 5648.

S9. C. Lee, W. Yang, R. G. Parr, *Phys. Rev. B* **1998**, 37**,** 785.

S10. K. Refson, *Comp. Phys. Comm.* **2000**, 126**,** 310.

S11. C. Hoheisel, A. Wurflinger, *J. Chem. Phys.* **1989**, 91, 473.

S12. M. Wulff, S. Bratos, A. Plech, R. Vuilleumier, F. Mirloup, M. Lorenc, Q. Kong, H. Ihee, *J. Chem. Phys.* **2006**, 124, 034501.

S13. S. Bratos, F. Mirloup, R. Vuilleumier, M. Wulff, A. Plech, *Chem. Phys.* **2004**, 304, 245.